TIME-DISTANCE HELIOSEISMOLOGY WITH THE MDI INSTRUMENT: INITIAL RESULTS

T. L. DUVALL JR.
Laboratory for Astronomy and Solar Physics, NASA Goddard Space Flight Center, Greenbelt, MD 20771, U.S.A.

A. G. KOSOVICHEV, P. H. SCHERRER, R. S. BOGART, R. I. BUSH, C. DE FOREST, J. T. HOEKSEMA and J. SCHOU
W. W. Hansen Experimental Physics Laboratory, Stanford University, Stanford, CA 94305, U.S.A.

J. L. R. SABA, T. D. TARBELL, A. M. TITLE and C. J. WOLFSON
Lockheed-Martin Advanced Technology Center, 91-30/252, 3251 Hanover St., Palo Alto, CA 94304, U.S.A.

P. N. MILFORD
Parallel Rules, Inc., 41 Manzanita Ave., Los Gatos, CA 95030, U.S.A.

(Received 28 October, 1996; in revised form 20 November, 1996)

Abstract. In time-distance helioseismology, the travel time of acoustic waves is measured between various points on the solar surface. To some approximation, the waves can be considered to follow ray paths that depend only on a mean solar model, with the curvature of the ray paths being caused by the increasing sound speed with depth below the surface. The travel time is affected by various inhomogeneities along the ray path, including flows, temperature inhomogeneities, and magnetic fields. By measuring a large number of times between different locations and using an inversion method, it is possible to construct 3-dimensional maps of the subsurface inhomogeneities.

The SOI/MDI experiment on SOHO has several unique capabilities for time-distance helioseismology. The great stability of the images observed without benefit of an intervening atmosphere is quite striking. It has made it possible for us to detect the travel time for separations of points as small as 2.4 Mm in the high-resolution mode of MDI (0.6 arc sec pixel $^{-1}$). This has enabled the detection of the supergranulation flow. Coupled with the inversion technique, we can now study the 3-dimensional evolution of the flows near the solar surface.

1. Introduction

Three strong features of the MDI instrument on SOHO (Scherrer *et al.*, 1995) are the stability coming from the absence of an intervening atmosphere between the telescope and the Sun, an orbit in continuous sunlight enabling long sequences of 'around-the-clock' observing, and the relatively high resolution compared to some groundbased helioseismology experiments. In this paper, we describe work that fully exploits these features of MDI and which points to a future in which we will be able to follow in detail the subsurface convection.

We are using a new technique coming to be known as time-distance helioseismology (Duvall *et al.*, 1993, 1996a, b; Kosovichev, 1996; Kosovichev and Duvall, 1996; D'Silva, 1996; D'Silva *et al.*, 1996), in which the time $t(x_1, x_2)$ for acoustic waves to travel between different surface locations (x_1, x_2) is measured from a

Solar Physics **170:** 63–73, 1997.

cross-correlation technique. In the first approximation, the time $t(x_1, x_2)$ depends on inhomogeneities along a geometric ray path connecting the surface locations. If the temperature is locally high, the waves will traverse the region more quickly leading to a shorter travel time. If there is a flow with a component in the direction of the ray path, the flow will tend to speed up the wave in the direction of the flow, while slowing it down in the reciprocal direction. In this case, we are led to the very distinctive signature of the travel time being different for waves traveling in opposite directions between the same points. We have thought of no other effect which can yield this signature.

A magnetic field in the region of wave travel can also lead to travel time anisotropy (Duvall *et al.*, 1996a). This is somewhat harder to isolate, as the distinctive signature of the field is that waves travelling along the field direction have a different wave speed than waves travelling perpendicular to the field. For some field geometries, it is possible to set up pairs of rays that intersect at right angles to look for this type of signature, but it is more difficult as the two rays have different paths except at the location where they intersect, and so other inhomogeneities can confuse the issue. The general form of rays below the surface is shown in Figure 5. In this paper the effect of magnetic anisotropy is not considered, because we have studied a very quiet region.

2. Observations

For this study we have used 8.5 hours of Doppler images from January 27, 1996 taken in the high-resolution mode of MDI, which has 0.6 arcsec pixel^{-1}. To study convection near the surface, it is necessary to use fairly short time intervals in order that the evolution not be too great during the observing interval. On the other hand, it is necessary to observe for some length of time in order to get a statistical sample of waves. The 8.5 hours is a compromise between these two competing requirements, with the supergranule lifetime of about 1 day putting an upper limit on how long to observe. Another point is that we need to observe for longer than the travel time, since the correlation that we are detecting arises from the same wave traveling from one location to the other through the subsurface layers. The travel times used in the present study are for surface point separations in the range 6-30 Mm, and are in the range 17–34 min.

An example of a Doppler image is shown in Figure 1. There is considerable high spatial frequency information in the image, as measurements of the point-spread function of the instrument would predict (Scherrer *et al.*, 1995). And in fact, with 0.6 arc sec pixel^{-1} we are somewhat oversampling the p-mode signal. With this sampling the spatial Nyquist frequency is near spherical harmonic degree $l = 5000$. But the fundamental mode, the lowest frequency mode in the p-mode range, crosses the peak acoustic cutoff frequency ($\sim$ 5.3 mHz) at degree $l = 2700$. Since the peak of the power envelope is near temporal frequency 3.2 mHz, there is very little power

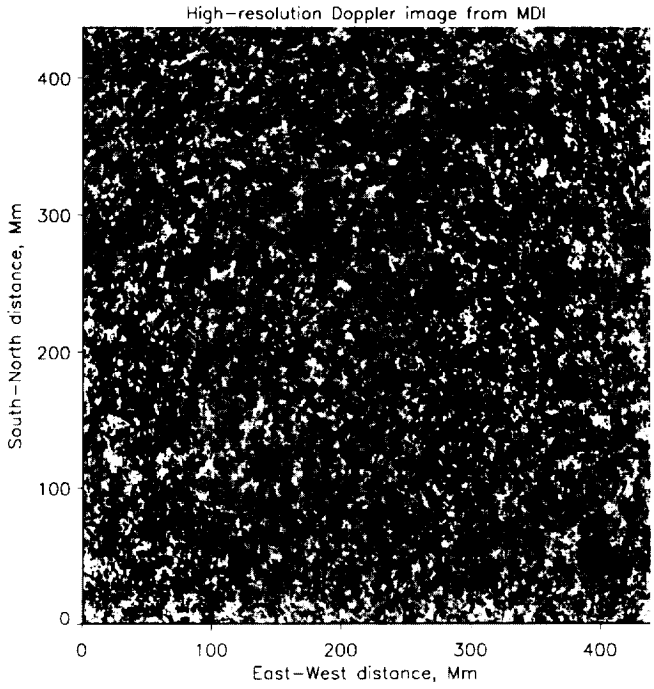

Figure 1. A MDI Dopplergram for the high-resolution field on 27 January, 1996. White is for receding velocity, black for approaching. The solar rotation has been removed. The image is dominated by the p-mode oscillations and granulation. The standard deviation of the velocity values is 244 m s^{-1}.

due to oscillations in the outer half (in spatial frequency) of the power spectrum. We have used this information explicitly in some later experiments in which the images are binned 2 × 2 on board the SOHO spacecraft to reduce the telemetry required.

The mean power spectrum of the 8.5 hours of data is shown in Figure 2. The spectrum is smooth, as it has been averaged over azimuth. The spatial frequency response has been flattened to remove the effects of the point-spread function. The excellent quality of the data is apparent. One striking thing is the large width of the f mode, which increases to ~1 mHz (full-width at half maximum) in width at $l = 2500$. It seems likely that much of this width could be caused by motions at the surface causing the waves to be Doppler shifted. Using the standard Doppler-shift relation, $v = \Delta\omega/k$, we find a flow velocity, v, of 0.9 km s^{-1} for a frequency shift, $\Delta\omega/2\pi$, of 0.5 mHz (one half of full-width at half maximum), and for a horizontal wave number, $k = \sqrt{l(l+1)}/R_\odot$. This is of the order of surface motions from convection, as determined by correlation tracking or as we find later in this paper by the time-distance technique.

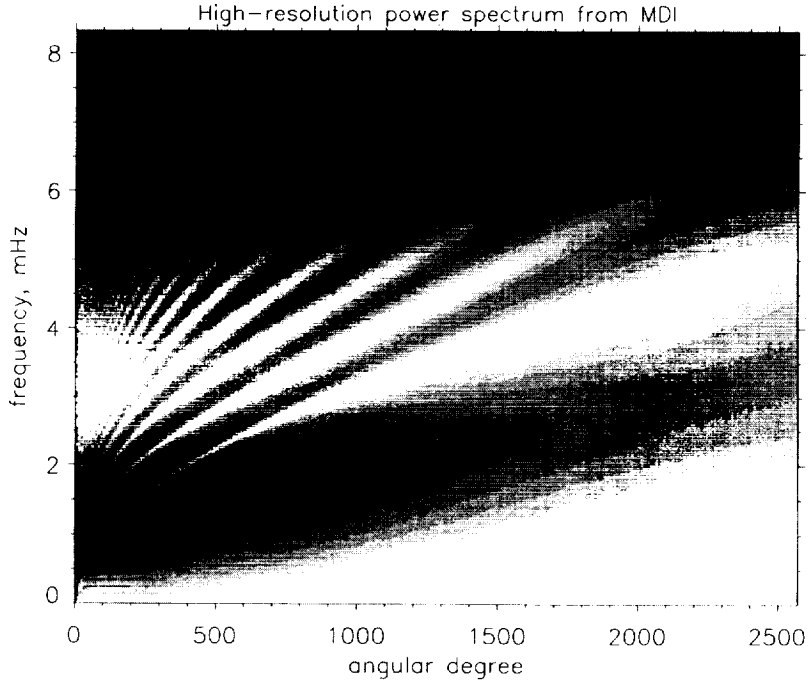

Figure 2. A mean power spectrum for the 8.5 hour interval studied on 27 January, 1996. The solar rotation was removed before the power spectrum was computed. The raw data was binned 2×2 before the analysis, so the spatial Nyquist frequency shown is half of the maximum achievable, although we get almost all the oscillation signal with the present analysis. The power spectrum is smooth because it has been averaged over wave direction.

3. Analysis

To measure the travel times between different locations, we calculate the temporal cross-correlation function between the data at one location and the data within an annulus at some great-circle distance from the point. We look at both positive and negative lags of the correlation function, as this tells us in which direction the waves are travelling. For example, a signal at location 1 first and later at location 2 will lead to a lag signal of one sign while a signal first at location 2 will lead to a correlation at the opposite sign of lag.

The cross-correlation function, averaged over a number of origins, is shown in Figure 3, along with a curve showing the time versus distance for a simple theory. If we imagine generating a pulse of acoustic energy at the surface that propagates along the ray paths to the distant location, we might expect to see a pulse at the distant location. But in fact we see something that is much broader and really looks like a wave packet with a period of 5 min, and a width in time of about 1/bandwidth of our oscillation power spectrum, or $(1\ \text{mHz})^{-1} = 17$ min. This makes sense, because the pulse that we generated at the surface had an infinite

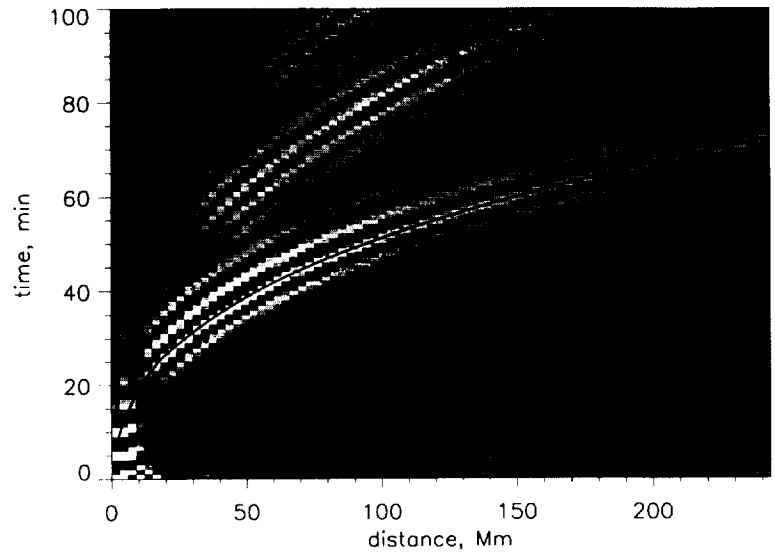

Figure 3. A mean cross-correlation function for the data. The solid line is a theoretical plot of the time for waves to travel along a ray path for the specified great-circle distance. The grayscale picture is the cross-correlation function. The first, second and third bounces are visible near 30 min, 60 min, and 90 min The fine structure in each of the ridges is caused by the finite bandpass of the oscillations.

bandwidth and so could make a zero-width feature in the correlation function. As shown earlier by Duvall *et al.* (1993), the correlation function that we observe is the Fourier transform of the power spectrum (e.g., Figure 2). The remaining features in Figure 3 correspond to the multiple bounces. If there is a correlation observed at time t and at distance d, there will be similar signals at $n \times t$ and $n \times d$, where n is integral. In the figure, the second and third bounces are seen.

For distances shorter than 10 Mm in Figure 3, we see a gap in the signal level and then some features parallel to the abscissa, which appear quite different to the wave packet type of feature present at larger distances. We hypothesize that the falloff of signal below 10 Mm distance is caused by the relative paucity of high spatial-frequency signal in the raw signal (note that the spectrum in Figure 2 has had the high spatial power corrected, while this has not been done to the data in Figure 3). We also hypothesize that the large signal in the neighborhood of the origin is caused by long wavelength features. To get around these problems and to separate adequately the first and second skip at short distances, we have used cross-correlations that have been filtered in phase speed (ω/k) with a fairly narrow bandpass. An example of one of these cross-correlations, covering the distance range 4.7-8.3 Mm, is shown in Figure 4. Our problems with lack of time-distance signal at short distances and spurious signals would appear to be solved.

In some earlier work (Duvall *et al.*, 1993), the correlation function was rectified by using the analytic signal formalism, and times were measured from this signal,

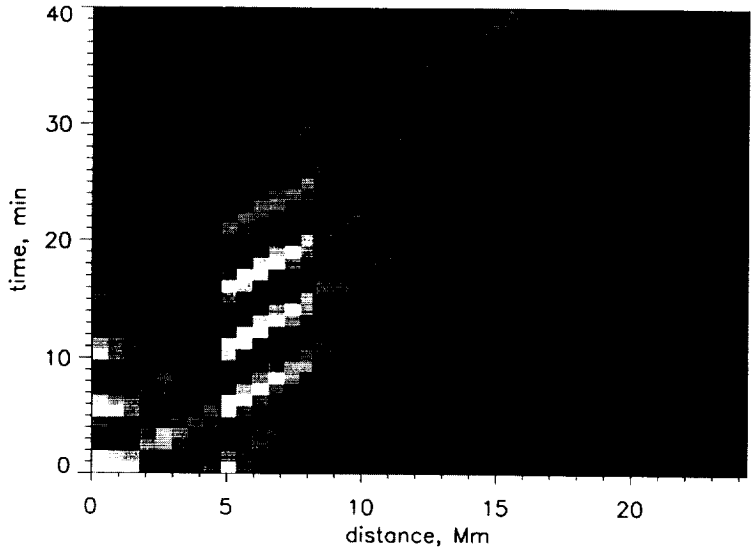

Figure 4. Cross-correlation function after bandpass filtering in phase velocity. The signal in the target distance range is enhanced.

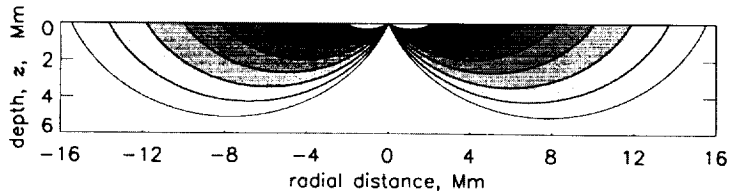

Figure 5. The rays going from the center to the different annuli. The ray paths are curved because of the increasing sound speed with depth. The sound speed increases from 7 km s^{-1} near the surface to 35 km s^{-1} at 10 Mm depth. The horizontal separation between surface points is approximately π times the depth. The measured travel times are sensitive to the component of velocity along the particular ray path.

which is the envelope of the correlation function. Later it was found that the higher frequency structure in the correlation function is actually a more sensitive measure of subsurface inhomogeneities (Duvall *et al.*, 1996a). In that work, the location of one of the fine-structure peaks was determined by measuring the zero crossing of the instantaneous phase of the correlation function. For the present work, this has been further refined (Kosovichev and Duvall, 1996). A 20-min interval in the neighborhood of the peak in the correlation function is fit to a Gaussian wave packet, with independent parameters for the location of the envelope, the location of one of the fine-structure peaks, the amplitude and width of the Gaussian, and the frequency. All the results shown are from the location of the fine-structure peak.

In Figure 5, we show some examples of raypaths below the surface. The ray paths are curved because of the increasing sound speed with depth in the Sun.

A useful rule of thumb is roughly that the horizontal distance between surface reflections is π multiplied by the depth of the turning point of the ray. Also the length along the ray path is four times the depth. These relations are exactly true for a polytrope and approximately true for a real solar model.

Following Duvall *et al.* (1996a), we compute the mean cross-correlation for waves travelling both out from the center to the annuli and the reverse. The difference of the times measured from these cross-correlations is a measure of divergence of the flow. It could be due to either a downflow near the central location or to an average horizontal outflow (or inflow) near the annulus. In addition to this divergence signal, a mean time is computed for the inward and outward waves.

To get more directional information about flows, we divide the annulus surrounding a point into quadrants centered on the four directions north, south, east, west (Duvall *et al.*, 1996b). The signals from the four quadrants are cross-correlated separately with the signal from the central point. The positive and negative temporal lags of these four correlation functions (corresponding to the two directions of propagation) are separated, yielding 8 correlations in all. Pairs of these correspond to each of the four cardinal directions, e.g., waves going from the eastern quadrant to the central point and from the central point to the western quadrant. The average correlation function for each of the four directions is computed from these pairs. The travel times are measured from the first skip from these correlations. Signals proportional to a flow are obtained by taking the difference of eastward and westward times (and likewise the northward and southward times).

In Figure 6 we show the four different sets of times computed for each range of distance: (i) outward–inward, (ii) west–east, (iii) north–south, and (iv) mean time. These 32 images are the input to the inversion described below.

In general, the signals for smaller annuli should be more sensitive to near-surface inhomogeneities. The cellular pattern with the scale size of supergranulation is most apparent in the outward–inward signal. Of course, the rays focus at the center points at the surface, but also reach the surface in the annuli. One interesting thing to notice is the apparent large-scale patterns visible in the signals from the larger annuli. We cannot distinguish directly whether these patterns are due to large scale signals near the surface that are being picked by the annular filter or they are due to larger scale flows near the bottom of the ray paths visible because the rays for the larger annuli penetrate deeper. In principle the inversion is able to distinguish between these options, but it would be useful to have another way to see this. Maybe in future work the signal from the second bounce could be used to make this distinction.

To check that we are seeing something with a basis in reality, we have used the west–east and north–south signals for the smallest annulus to make an apparent horizontal velocity to compare with the mean Doppler image over the 8.5-hour period. The west–east and north–south times are taken as the components of a horizontal vector and the line-of-sight component of this vector is taken. The times are calibrated using the mean sound speed over the depth range of the rays from a solar model. The comparison between these two is shown in Figure 7. The very

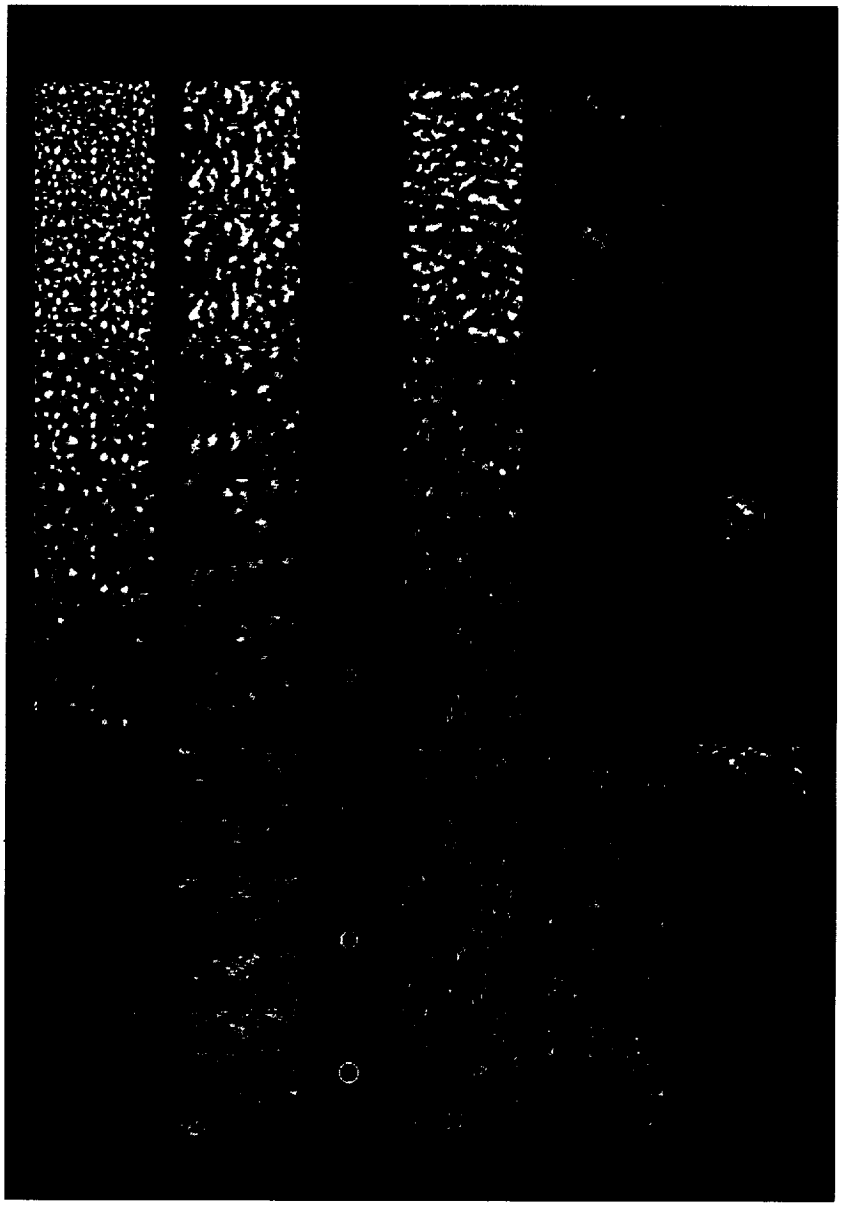

Figure 6. Maps of the times measured and input to the inversion procedure. The 8 pictures vertically are for the 8 different annulus sizes. The sizes of the annuli are shown in the central column, smallest at the top and largest at the bottom. The horizontal size of each image is 370 Mm. (a) Time for outward-going waves minus inward-going waves with white displayed as a negative signal. The r.m.s. signal in the top image is 0.2 min while in the bottom one is 0.04 min. (b) Westward times minus eastward times. The r.m.s. signal in the top image is 0.35 min while in the bottom image is 0.19 min. (c) Northward times minus southward times. The magnitudes are similar to b). (d) The variation in mean time for the average of inward and outward times with a negative signal displayed as white. The r.m.s. of the top image is 0.05 min while for the bottom image it is 0.08 min. A correlation of this signal with the location of the magnetic features can be seen, in agreement with results of Duvall *et al.* (1996a, b). (e) The magnetic field in this region, as observed with the MDI instrument. (f) The mean Doppler signal observed for the 8.5 hour interval. This shows mainly the horizontal motions of supergranules. Near the center of the disk (lower center of picture) the signal from horizontal flows disappears because it is perpendicular to the line of sight. The images in a single column are all on the same scale.

Figure 7. A comparison between a simulated Doppler image using the images from the top line of Figures 6(b) and 6(c) and the mean Doppler image for the 8.5 hours (Figure 6(f)). (a) The simulated image. The east–west and north–south times are combined and then projected onto the line of sight. (b) The mean Doppler image for the 8.5 hours.

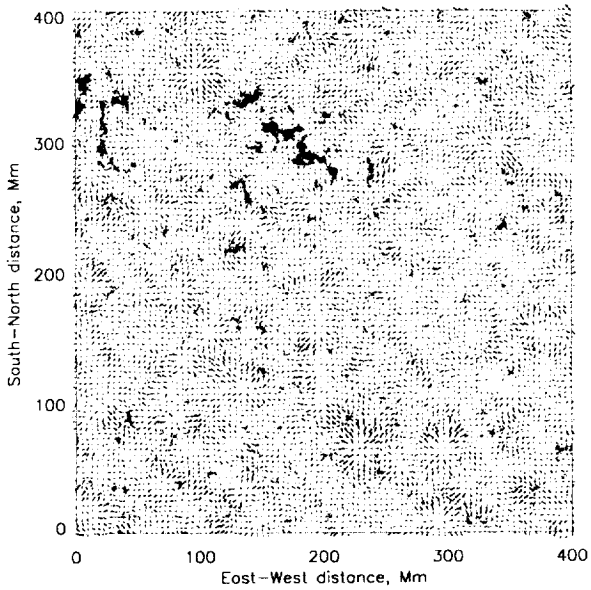

Figure 8. A comparison between the absolute value of magnetic field (in color) and the simulated surface velocity from the time-distance pictures (arrows). The longest arrow is for 1 km s^{-1} velocity.

high correlation is apparent. The correlation coefficient between these two images is 0.74. The signals disappear near the disk center because the supergranulation velocity is predominantly horizontal which is perpendicular to our line of sight at disk center.

Another check on our understanding is shown in Figure 8. The same components of east–west and north–south velocity used in Figure 7 are combined to show horizontal velocity vectors. The vectors are overlaid on an image of the absolute value of magnetic field. We see that the magnetic field tends to lie at the boundaries

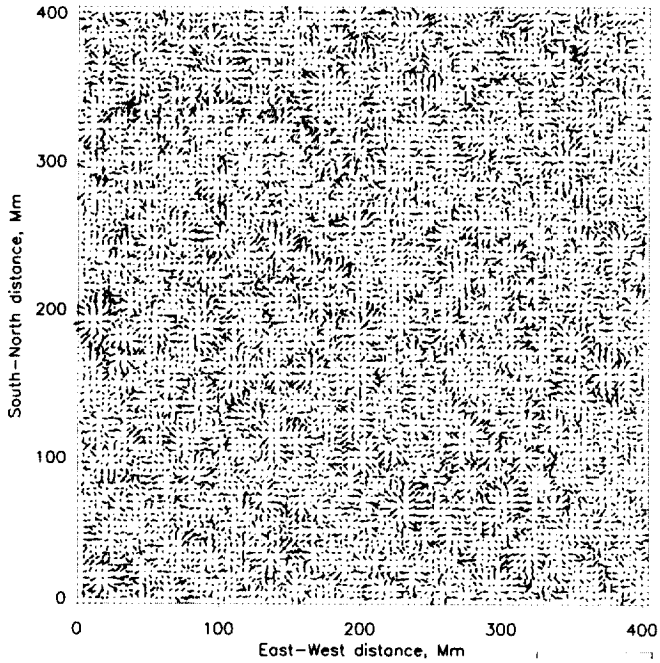

Figure 9. The horizontal flows near the surface from the inversion procedure are shown as vectors. The vectors are overlaid on the inverted temperature structure shown in blue and red for hotter and cooler.

of the cellular outflows, in agreement with our general picture of the magnetic network.

The time – distance maps are used in a ray-theory inversion (Kosovichev, 1996; Kosovichev and Duvall, 1996). The region of the Sun is separated into a 3-D grid of inhomogeneities with the same horizontal sampling interval as the input images (4.3 Mm) and an equal increment in depth covering the same depth range as the input data. The number of grid points in depth is taken to be the same as the number of input images (in this case, 8). Each 3-D grid point has four independent variables, the three components of flow velocity and a sound speed inhomogeneity. No attempt is made to satisfy any conservation equations, such as the continuity equation.

In Figure 9, we show the inversion results for the surface layer. The high correlation with the mean Doppler image is apparent. One advantage of studying near-surface regions is that we do have extra information for comparison at the surface that we would not have for the deep interior.

In Figure 10 we present a vertical cut showing the subsurface flows and sound speed inhomogeneities. It would appear that the pattern of horizontal motions at the surface only persists to a few Megameters in depth. But it is probably still premature to draw strong conclusions because of the newness of the method.

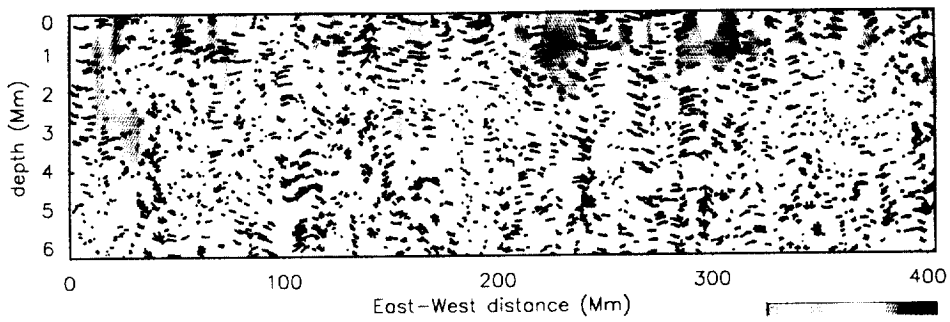

Figure 10. A vertical cut showing the component of flow in the plane. The flow is again shown as vectors and is overlaid on the temperature inhomogeneities.

4. Conclusions

We have shown that there is detailed information about the subsurface inhomogeneities contained in the helioseismology data. We have also shown it should be possible to extract this information and have shown some first-order attempts to do so. We would appear to have an exciting new window into the solar interior.

Acknowledgements

The authors acknowledge many years of effort by the engineering and support staff of the MDI development team at the Lockheed Palo Alto Research Laboratory (now Lockheed-Martin Advanced Technology Center) and the SOI development team at Stanford University. SOHO is a project of international cooperation between ESA and NASA. This research is supported by the SOI-MDI NASA contract NAG5-3077 at Stanford University.

References

D'Silva, S.: 1996, *Astrophys. J.* **469**, 964.
D'Silva, S., Duvall, T. L., Jr., Jefferies, S. M., and Harvey, J. W.: 1996, *Astrophys. J.* **471**, 1030.
Duvall, T. L., Jr., Jefferies, S. M., Harvey, J. W., and Pomerantz, M. A.: 1993, *Nature* **362**, 430.
Duvall, T. L., Jr., D'Silva, S., Jefferies, S. M., Harvey, J. W., and Schou, J.: 1996a, *Nature* **379**, 235.
Duvall, T. L., Jr., Kosovichev, A. G., Scherrer, P. H., and Milford, P. N.: 1996b, *Bull. Am. Astron. Soc.* **188**, 898.
Kosovichev, A. G.: 1996, *Astrophys. J.* **461**, L55.
Kosovichev, A. G. and Duvall, T. L., Jr.: 1996, in J. Christensen-Dalsgaard and F. Pijpers (eds.), 'Solar Convection and Oscillations and their Relationship', *Proc. of SCORe'96 Workshop*, Aarhus, Denmark, May 27–31, 1996, Kluwer Academic Publishers, Dordrecht, Holland, in press.
Scherrer, P. H., Bogart, R. S., Bush, R. I., Hoeksema, J. T., Kosovichev, A. G., Schou, J., Rosenberg, W., Springer, L., Tarbell, T. D., Title, A., Wolfson, C. J., Zayer, I., and the MDI Engineering Team: 1995, *Solar Phys.* **162**, 129.